NACA TN 3059

NATIONAL ADVISORY COMMITTEE FOR AERONAUTICS

TECHNICAL NOTE 3059

ELASTIC BUCKLING UNDER COMBINED STRESSES OF FLAT PLATES WITH INTEGRAL WAFFLE-LIKE STIFFENING

By Norris F. Dow, L. Ross Levin, and John L. Troutman

Langley Aeronautical Laboratory
Langley Field, Va.

Washington
January 1954

NATIONAL ADVISORY COMMITTEE FOR AERONAUTICS

TECHNICAL NOTE 3059

ELASTIC BUCKLING UNDER COMBINED STRESSES OF FLAT PLATES WITH INTEGRAL WAFFLE-LIKE STIFFENING

By Norris F. Dow, L. Ross Levin, and John L. Troutman

SUMMARY

Theory and experiment were compared and found in good agreement for the elastic buckling under combined stresses of long flat plates with integral waffle-like stiffening in a variety of configurations. For the buckling of such flat plates, 45° waffle stiffening was found to be the most effective of the configurations for the proportions considered over the widest range of combinations of compression and shear.

INTRODUCTION

"The advantages claimed for integral construction," reference 1 states, "are potential increase of structural efficiency, reduced assembly time, and the maintenance of a smooth outer surface." Despite the pessimism of reference 1 concerning the cost of the machinery and plant facilities for the production of integrally stiffened construction, these facilities are becoming available both in this country (ref. 2) and abroad (ref. 3), and research effort continues to be directed toward the achievement of what reference 1 calls "the spectacular as regards structural efficiency."

In reference 4, the use of relatively shallow integral waffle-like stiffening was shown experimentally to produce substantial increases in the elastic longitudinal compressive buckling stresses of long flat plates, particularly when two-way ribbing inclined at -45° + 45° to the sides of the plate was used. No attempt was made in reference 4 to correlate the experimental results with theoretical predictions because no theory was then available for the calculation of the characteristics of integral waffle-like stiffening. Such a theory has now become available (ref. 5) and the purpose of the present paper is first to show that this theory, together with available theories for the elastic buckling of orthotropic

flat plates, is adequate to predict the results of reference 4 and additional experimental results reported herein for elastic buckling under combined stresses, and second to survey the relative effectiveness of various stiffening configurations as shown by the theories.

No claim is advanced regarding the spectacularity of these results, but as even the author of reference 1 finally concludes, and the discussion of his paper (ref. 6) emphasizes, "There is no doubt, however, that . . . (integrally stiffened) . . . material is well worth while and could be used to advantage in a wide range of applications."

SYMBOLS

b_w	height of rib (web), in.
D_1	longitudinal bending stiffness, in.-kips
D_2	transverse bending stiffness, in.-kips
D_k	longitudinal or transverse twisting stiffness, in.-kips
E	Young's modulus, taken as 10.5×10^3 ksi for 355-T61 aluminum alloy
H	overall thickness, skin plus ribs, in.
k_c	coefficient in plate-buckling formula for compression
k_s	coefficient in plate-buckling formula for shear
L	length of plate, in.
N_x	longitudinal compressive loading, kips/in.
N_{xy}	shear loading, kips/in.
$\bar{t}$	thickness of equal-weight solid plate, in.
t_s	skin thickness, in.
W	plate width, in.
γ	shear strain

ϵ	compressive strain
θ	angle of skew of ribbing, deg
μ	Poisson's ratio, taken as 0.32 for 355-T61 aluminum alloy
μ_y	Poisson's ratio associated with bending
σ	compressive stress, ksi
σ_{cy}	compressive yield stress, ksi
τ	shear stress, ksi

TEST SPECIMENS AND PROCEDURE

The test specimens used for this investigation included those of reference 4 and an additional series similar to those of reference 4 but having minor variations for testing under combined stresses. All these specimens were square tubes approximately 10 inches wide by 45 inches long made up of four integrally stiffened flat plates fabricated as sand castings of 355 aluminum alloy which had been heat-treated and aged according to recommended procedures (ref. 7 or 8) to produce the T61 condition. The castings were machined to the desired thicknesses and riveted together using corner angles of 24S-T4 aluminum alloy and 3/32-inch-diameter A17S-T4 aluminum-alloy rivets at approximately 1/2-inch pitch with the ribbing on the outside on all four sides of the tube. The corner angles were 1/16 × 1/2 × 1/2 for the compression specimens and 1/16 × 3/4 × 3/4 for all other specimens. For the latter, two rows of rivets were used along each angle leg, and, in addition, the angles were cemented to the castings with Araldite cement in order to carry the shear stresses around the corners of the tubes. Nine configurations of integral stiffening were used (see fig. 1), namely longitudinal ribbing, two-way ribbing at -15° + 15°, -30° + 30°, -45° + 45°, -60° + 60°, and -75° + 75° to the longitudinal axis of the specimen, transverse ribbing, longitudinal and transverse ribbing, and combined -30° + 30° skewed and transverse ribbing. On all specimens the nominal rib cross-sectional dimensions were the same (see fig. 2). The rib spacing, measured as the perpendicular distance between parallel ribs, was 1/2 inch on the longitudinally or transversely stiffened plates, and 1 inch on all the others except the -30° + 30° + 90° ribbing for which a $1\frac{1}{2}$-inch spacing was used. These spacings were such as to keep the ribbing material approximately equal in weight to sheet 0.050 inch thick. Also on all specimens, except in the series of tests of plates with -45° + 45° ribbing in which the skin thickness was varied, the

nominal skin thickness t_s was 0.050 inch. For the series in which t_s was varied, nominal skin thicknesses of 0.025, 0.050, 0.075, and 0.100 inch were used.

The compression specimens were tested flat-ended in the 1,200,000-pound-capacity testing machine. All other specimens were tested with their ends bolted solidly to end fixtures, which reduced the unsupported test length by approximately 5 inches, in the combined load testing machine of the Langley structures research laboratory (see fig. 3). Buckling was detected by "buckle-bars" resting against the sides of the tubes, as was done in reference 4.

By preselection of the combinations of longitudinal compression and shear applied, every effort was made to keep the buckling stresses within the elastic range. For some stiffening configurations, plastic buckling (as will be discussed in a subsequent section) was not completely avoided, in large measure because the material properties achieved were substantially below the handbook values for 355-T61 (see ref. 7 or 8). Compression and shear stress-strain curves measured for samples of the specimen material are presented in figure 4; the measured value of compressive yield stress was only 28 ksi compared to the typical value to be expected of 37 ksi.

Dimensions of specimens and test data are given in table 1.

THEORETICAL ANALYSIS

Elastic longitudinal compressive buckling loads for the test specimens were calculated from the formula of reference 9

$$N_x = \frac{\pi^2}{W^2}\left[\left(k_c - 2\right)\sqrt{D_1 D_2} + 4D_k + 2\mu_y D_1\right] \qquad (1)$$

where

N_x longitudinal compressive loading, kips/in.

W plate width, in.

D_1, D_2, μ_y, D_k elastic constants for the proportions and nominal dimensions of the test specimens as given by the formulas of reference 5 (experimentally measured values of the coefficients α and β of those formulas were used)

k_c compressive buckling coefficient, determined in the manner of reference 9 from a curve (such as that of figure 1(b) of ref. 10) of compressive buckling coefficient against plate aspect ratio for an isotropic flat plate having loaded edges fixed and unloaded edges simply supported. (It is shown in ref. 9 that such a curve may be used for orthotropic plates if the aspect ratio is calculated as an "effective aspect ratio" equal to $\frac{L}{W}\sqrt[4]{\frac{D_2}{D_1}}$.)

Elastic shear buckling loads for the test specimens were calculated from the formula of reference 11

$$N_{xy} = \frac{\pi^2}{W^2}\left(k_s\sqrt[4]{D_1 D_2^3}\right) \tag{2}$$

where

N_{xy} shear loading, kips/in.

k_s shear buckling coefficient, determined from curves of shear buckling coefficient plotted against the inverse of the "effective aspect ratio" as defined for compression. Such curves, similar to those of reference 11 but for short edges clamped and long edges simply supported, are presented in figure 5.

Reductions in calculated buckling loads to allow for plasticity were made as follows:

(1) An "effective" or "equivalent" stress-strain curve was derived from the material stress-strain curve such that the ratio of ordinates of the derived and material curves at the same strain was the same as the ratio of axial stiffness of unit-width integrally stiffened plate to axial stiffness of unit-width solid plate of equal weight.

(2) The secant modulus of this reduced stress-strain curve at the calculated elastic buckling strain was used as the effective modulus in the buckling equations. The buckling strain was calculated as $\frac{N_x/\bar{t}}{E}$ times the inverse ratio of axial stiffness of unit-width integrally stiffened plate to axial stiffness of unit-width solid plate of equal weight.

The elastic longitudinal compressive buckling loads calculated for the test specimens are plotted as the solid curves in figures 6(a) and 7(a), and the corresponding elastic shear buckling loads as the solid curves in figures 6(b) and 7(b). The corresponding plastic buckling loads are plotted as the dashed curves in the same figures. The results of the calculations are also given in table 1.

For combined longitudinal compression and shear, the buckling loads (both elastic and plastic) for the test specimens were calculated assuming a parabolic interaction curve between longitudinal compression and shear buckling as recommended in reference 12 for built-up square tubes. The results of these calculations are plotted as the solid curves (elastic) and dashed curves (plastic) in figure 8.

For comparisons of the relative effectiveness of the various stiffening configurations considered, calculations were also made for the buckling under combined stresses of infinitely long, simply supported integrally stiffened flat plates having the nominal specimen dimensions. These calculations were the same as those carried out for the finite length, fixed-ended test specimens except that values of k_c and k_s corresponding to infinite values of $\frac{L}{W}\sqrt[4]{\frac{D_2}{D_1}}$ were used.

The results of these calculations for infinitely long plates are presented in table 1 and figure 9.

CORRELATION OF THEORY AND EXPERIMENT

The test results, tabulated in table 1, are plotted as the circles and squares in figures 6 and 7 for simple longitudinal compression or shear loadings and in figure 8 for combined stresses as well. In the elastic range, as shown by the general coincidence of solid curves, dashed curves, and points, correlation between the calculated curves and the test points is generally as good as can be expected in view of the inherently poor dimensional tolerances of sand castings. Beyond the elastic range (where solid and dashed curves diverge), the test results correlate well in some cases with the calculated plastic values; in other cases the correlation is better if no reduction for plasticity is made. Accordingly, while the calculations of the elastic buckling loads appear to be confirmed by the data, no confirmation is made of the calculation of plastic buckling loads. Evidently in the plastic range variations in material properties from casting to casting in addition to the variations in cast dimensions increased the experimental scatter. If, for example, those specimens which achieved stresses comparable to the calculated elastic values were constructed of material having properties comparable to the typical handbook values (refs. 7 and 8) for 355-T61 aluminum alloy, they should have buckled elastically, and the stresses which

they achieved would be in confirmation of the calculations. Buckling loads even below those represented by the dashed curves of figures 6, 7, and 8 might be expected, on the other hand, if the material properties of some specimens were even lower than those measured and presented in figure 4. Possibly in this category were the three specimens represented by the square test points in figures 6, 7, and 8, namely the $-45^\circ + 45^\circ$ specimens having a skin thickness of 0.075 inch loaded in compression, and the $-30^\circ + 30^\circ + 90^\circ$ specimen loaded in shear. The buckling loads for these specimens were substantially below even the calculated plastic buckling loads. However, because joint failure occurred in all of these specimens, and only in these specimens (see also ref. 4), improper corner attachments would appear to be a more probable cause of the reductions in buckling loads for these specimens than low material properties.

COMPARISON OF EFFECTIVENESS OF VARIOUS STIFFENING CONFIGURATIONS AS LONG FLAT PLATES

A comparison of the relative effectiveness of the various stiffening configurations considered for resisting buckling under various combinations of longitudinal compression and shear as long flat plates in the elastic range is given in figure 9. Here are plotted interaction curves calculated from equations (1) and (2) as previously described.

The curves of figure 9 indicate that, of the configurations considered, the $-45^\circ + 45^\circ$ pattern is the most effective for pure longitudinal compression and the $-60^\circ + 60^\circ$ pattern is the most effective for pure shear. Further, there is evidently little merit in configurations having angles of skew of the ribbing greater than 60°. The effectiveness of such configurations is smaller (even in the elastic range), for all combinations of longitudinal compression and shear stress, than for angles of 60° or less.

Beyond the elastic range, angles of skew greater than 60° would become relatively even less effective. In fact, clearly the more plastic the stresses, the more nearly the angles of skew must conform, for greatest effectiveness, to the angles of principal stresses; that is, for longitudinal compression the angles will approach 0°, for shear the angles will approach 45° (see, for example, the dashed curve of figure 6(b) which indicates that, for the amount of plastic action allowed for in the calculations associated with the test specimens, the $-45^\circ + 45^\circ$ configuration is approximately as effective as the $-60^\circ + 60^\circ$ configuration).

The $0^\circ + 90^\circ$ and the $-30^\circ + 30^\circ + 90^\circ$ configurations show no outstanding characteristics in the elastic range (see fig. 9). In the plastic range, however, the $0^\circ + 90^\circ$ configuration should become relatively more

effective in compression, and the $-30^\circ + 30^\circ + 90^\circ$ configuration should become relatively more effective in both compression and shear. Accordingly, as a kind of compromise, the latter pattern may have at least a limited range of efficient application.

Square-pattern ribbing emerges as the most effective of the patterns considered for the widest range of loading conditions. Oriented at 45°, it is the most effective in the elastic range for longitudinal compression, as it undoubtedly is high in the plastic range for shear. Rotated to the $0^\circ + 90^\circ$ orientation it can be expected to become more effective high in the plastic range in compression, and, correspondingly, rotated to the $\pm 30^\circ \mp 60^\circ$ orientation it can be expected (see ref. 13) to become more effective in the elastic range for shear (in the latter case, attention must be paid to the direction of the shear stress in the selection of the plus and minus directions).

CONCLUDING REMARKS

Experiments on cast specimens have indicated that available theories are adequate for the prediction of elastic buckling of flat plates with integral waffle-like stiffening. Calculations based on the available theories show that, for the buckling of long flat plates for a wide range of loading conditions, integral waffle-like stiffening of the general proportions considered is most effective in a square pattern. The optimum orientation of the square pattern varies somewhat with the loading conditions, but a $-45^\circ + 45^\circ$ orientation has the most universal application.

Because of the coupling actions associated with one-sided stiffening, distortions other than those due to buckling may be of importance for some applications. Coupling becomes of greater significance as the depth and thickness of ribbing increases relative to the skin thickness. Particularly, if conditions of continuity at the edges of the plate are not such as to reduce the coupling distortions, the magnitude of these distortions, determined from the elastic constants of the plate, should be examined before ribbing relatively deeper or thicker than has been investigated is used.

Langley Aeronautical Laboratory,
National Advisory Committee for Aeronautics,
Langley Field, Va., October 8, 1953.

REFERENCES

1. Keen, E. D.: Integral Construction - Its Application to Aircraft Design and Its Effect on Production Methods. Jour. R.A.S., vol. 57, no. 508, Apr. 1953, pp. 215-227.

2. Anon.: Big Doings Mark Coming of Monster Presses. SAE Jour., vol. 61, no. 5, May 1953, pp. 31-37.

3. Anon.: Skins From the Solid. Aircraft Engineering, vol. XXIV, no. 286, Dec. 1952, pp. 361-363.

4. Dow, Norris F., and Hickman, William A.: Preliminary Experiments on the Elastic Compressive Buckling of Plates With Integral Waffle-Like Stiffening. NACA RM L52E05, 1952.

5. Dow, Norris F., Libove, Charles, and Hubka, Ralph E.: Formulas for the Elastic Constants of Plates With Integral Waffle-Like Stiffening. NACA RM L53E13a, 1953.

6. Anon.: Integral Construction - Report of the Discussion on the paper by E. D. Keen (published in the April Journal). Jour. R.A.S., vol. 57, no. 511, July 1953, pp. 461-462.

7. Anon.: Alcoa Aluminum and Its Alloys. Aluminum Co. of America, 1950.

8. Anon.: The Aluminum Data Book. Reynolds Metals Co. (Louisville), 1950.

9. Wittrick, W. H.: Correlation Between Some Stability Problems for Orthotropic and Isotropic Plates Under Bi-Axial and Uni-Axial Direct Stress. Aeronautical Quarterly, vol. IV, pt. I, Aug. 1952, pp. 83-92.

10. Stowell, Elbridge Z., Heimerl, George J., Libove, Charles, and Lundquist, Eugene E.: Buckling Stresses for Flat Plates and Sections. Proc. A.S.C.E., vol. 77, separate no. 77, July 1951, pp. 1-31.

11. Seydel, Edgar: The Critical Shear Load of Rectangular Plates. NACA TM 705, 1933.

12. Peters, Roger W.: Buckling Tests of Flat Rectangular Plates Under Combined Shear and Longitudinal Compression. NACA TN 1750, 1948.

13. Thielemann, Wilhelm: Contribution to the Problem of Buckling of Orthotropic Plates, With Special Reference to Plywood. NACA TM 1263, 1950.

TABLE 1.- DIMENSIONS OF TEST SPECIMENS, AND VALUES OF MEASURED AND CALCULATED BUCKLING LOADS

Stiffening arrangement, deg	Skin thickness, t_s in.	Overall thickness, H in.	Plate width, W in.	Thickness of equiv. plate, $\bar{t}$ in. (a)	Measured buckling loads, N_x, kips/in.	Measured buckling loads, N_{xy}, kips/in.	Calc. elastic buckling loads, N_x, kips/in.	Calc. elastic buckling loads, N_{xy}, kips/in.	Calc. plastic buckling loads, N_x, kips/in.	Calc. plastic buckling loads, N_{xy}, kips/in.	Calc. equiv. buckling stresses as long flat plates, $\frac{N_x}{\bar{t}}$ ksi (b)	Calc. equiv. buckling stresses as long flat plates, $\frac{N_{xy}}{\bar{t}}$ ksi (b)
0	0.053	0.255	10.1	0.106	0.49	0	[b]0.43	0	[b]0.43	0	3.73	0
	.039	.246	10.2	.103	.52	0	0	[b]0.29	0	[b]0.29	0	2.35
	.058	.247	10.1	.106	0	0.26						
	.052	.251	10.1	.110	0	.32						
					.12	.24						
					.25	.19						
					.30	.16						
-15 + 15	.060	.257	10.0	.108	.66	0	[b].65	0	[b].65	0	5.75	0
	.050	.245	10.0	.101	.59	0	0	[b].45	0	[b].45	0	3.72
	.053	.249	9.9	.107	0	.60						
-30 + 30	.066	.251	10.2	.106	.98	0	[b]1.12	0	[b]1.11	0	11.0	0
	.055	.249	10.2	.104	.90	0	0	[b].79	0	[b].77	0	9.10
	.049	.249	10.2	.098	.47	.61						
	.052	.246	10.2	.105	.57	.63						
-45 + 45	.038	.224	10.0	.080	.91	0	[c]1.06	0	[c].82	0		
	.037	.224	10.0	.080	.82	0	0	[c]1.29	0	[c].93		
	.028	.224	10.0	.076	0	.79						
-45 + 45	.062	.252	10.0	.101	1.22	0	[b]1.38	0	[b]1.25	0	14.2	0
	.056	.247	10.0	.101	1.27	0	0	[b]1.63	0	[b]1.25	0	17.3
	.046	.250	10.0	.097	.81	.58						
	.046	.249	10.0	.091	.81	.70						
	.047	.249	10.0	.099	0	1.18						
-45 + 45	.071	.271	10.1	.119	1.28	0	[d]1.76	0	[d]1.59	0		
	.079	.289	10.1	.128	1.21	0	0	[d]2.13	0	[d]1.54		
	.069	.274	10.0	.123	0	1.52						
-45 + 45	.096	.296	10.1	.147	1.78	0	[e]2.44	0	[e]2.26	0		
	.101	.296	10.1	.148	1.86	0	0	[e]2.96	0	[e]2.13		
	.089	.297	10.1	.145	0	1.86						
-60 + 60	.057	.248	10.1	.101	.99	0	[b]1.10	0	[b]1.05	0	11.0	0
	.059	.247	10.1	.103	.95	0	0	[b]1.91	0	[b]1.26	0	19.7
	.051	.248	10.2	.105	.97	.77						
	.055	.250	10.2	.106	.72	1.03						
-75 + 75	.051	.248	9.8	.098	.68	0	[b].60	0	[b].60	0	5.75	0
	.049	.245	9.8	.097	.63	0	0	[b]1.55	0	[b]1.03	0	15.6
	.051	.250	9.7	.106	.47	.92						
90	.044	.245	10.0	.113	.45	0	[b].36	0	[b].36	0	3.73	0
	.046	.248	10.1	.112	.49	0	0	[b]1.16	0	[b].78	0	12.4
	.060	.252	10.1	.114	0	.75						
	.058	.252	10.1	.117	.30	.59						
0 + 90	.067	.249	10.1	.111	.92	0	[b].94	0	[b].94	0	8.18	0
	.061	.250	10.1	.104	.83	0	0	[b]1.48	0	[b].93	0	13.7
	.045	.250	10.1	.097	.42	.64						
	.050	.250	10.1	.098	0	.93						
-30 + 30 + 90	.050	.247	10.3	.111	.96	0	[b]1.18	0	[b]1.17	0	9.32	0
	.050	.248	10.3	.111	1.23	0	0	[b]1.66	0	[b]1.13	0	14.0
	.044	.243	10.3	.122	0	.67						
	.047	.250	10.3	.119	.56	.82						

[a]Determined by weight.
[b]Calculated from equations (1) and (2) for nominal dimensions with t_s = 0.050 in.
[c]Calculated from equations (1) and (2) for nominal dimensions with t_s = 0.025 in.
[d]Calculated from equations (1) and (2) for nominal dimensions with t_s = 0.075 in.
[e]Calculated from equations (1) and (2) for nominal dimensions with t_s = 0.100 in.

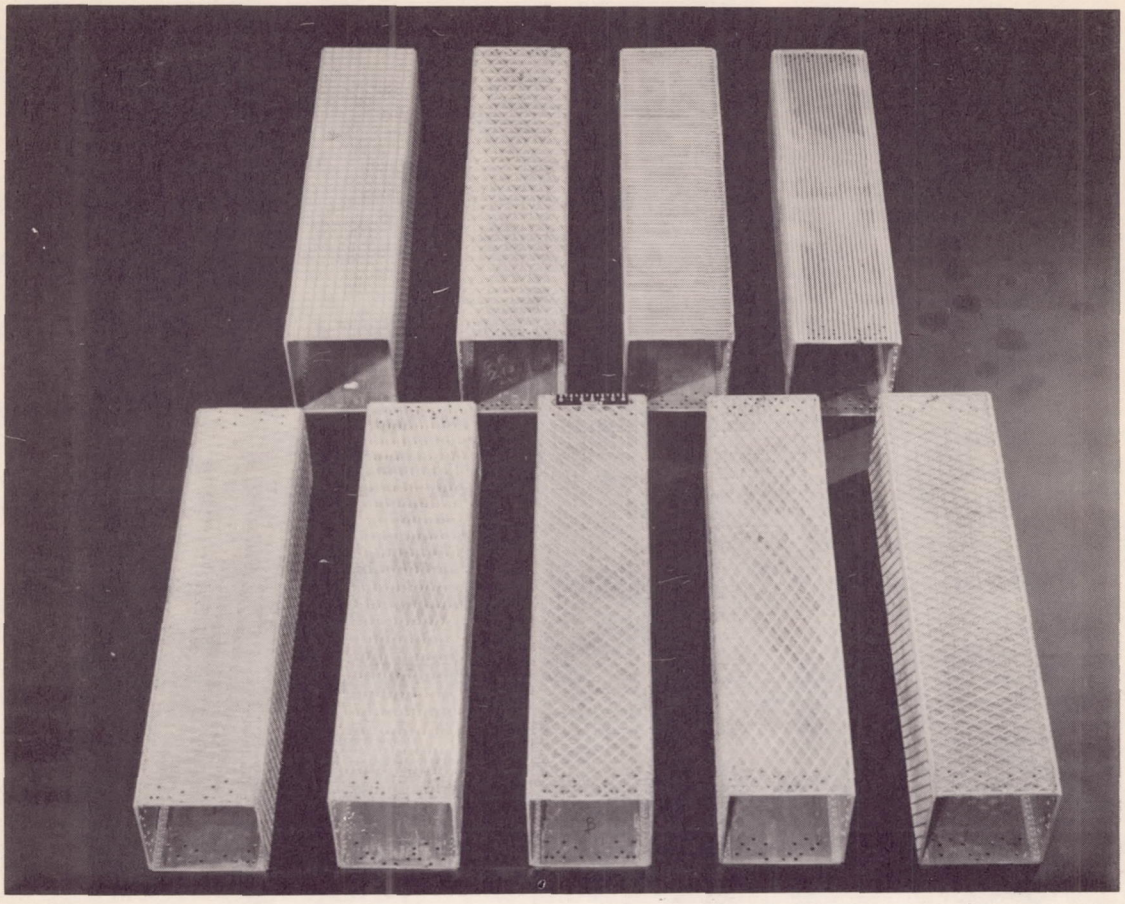

L-80644.1

Figure 1.- Ribbing configurations considered: top row, 0° + 90°, -30° + 30° + 90°, 90°, and 0°; bottom row, -75° + 75°, -15° + 15°, -45° + 45°, -30° + 30°, and -60° + 60°.

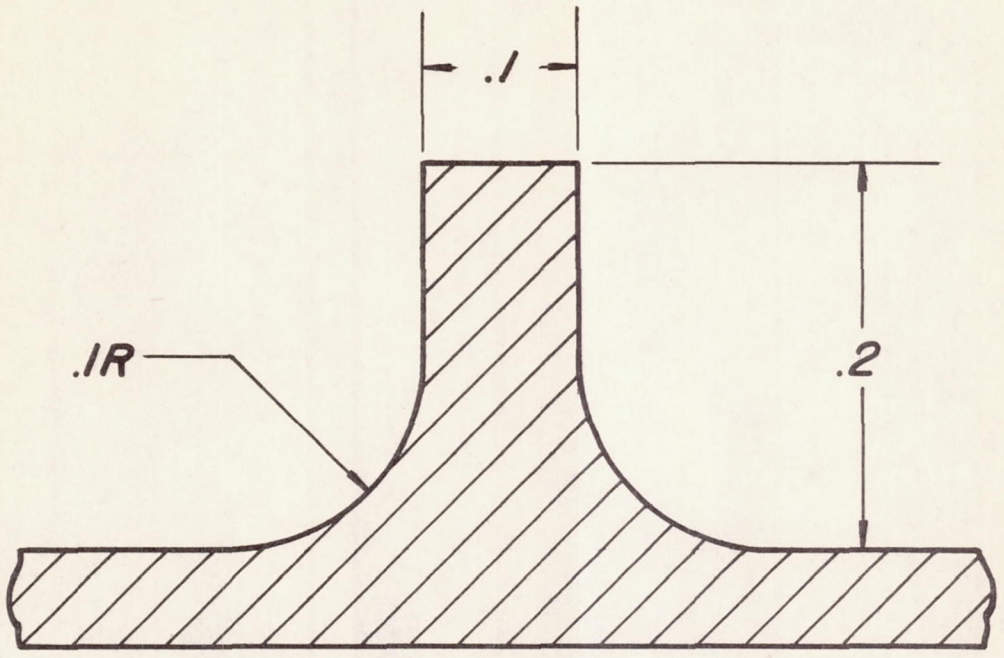

Figure 2.- Cross section of ribbing used on all test specimens.

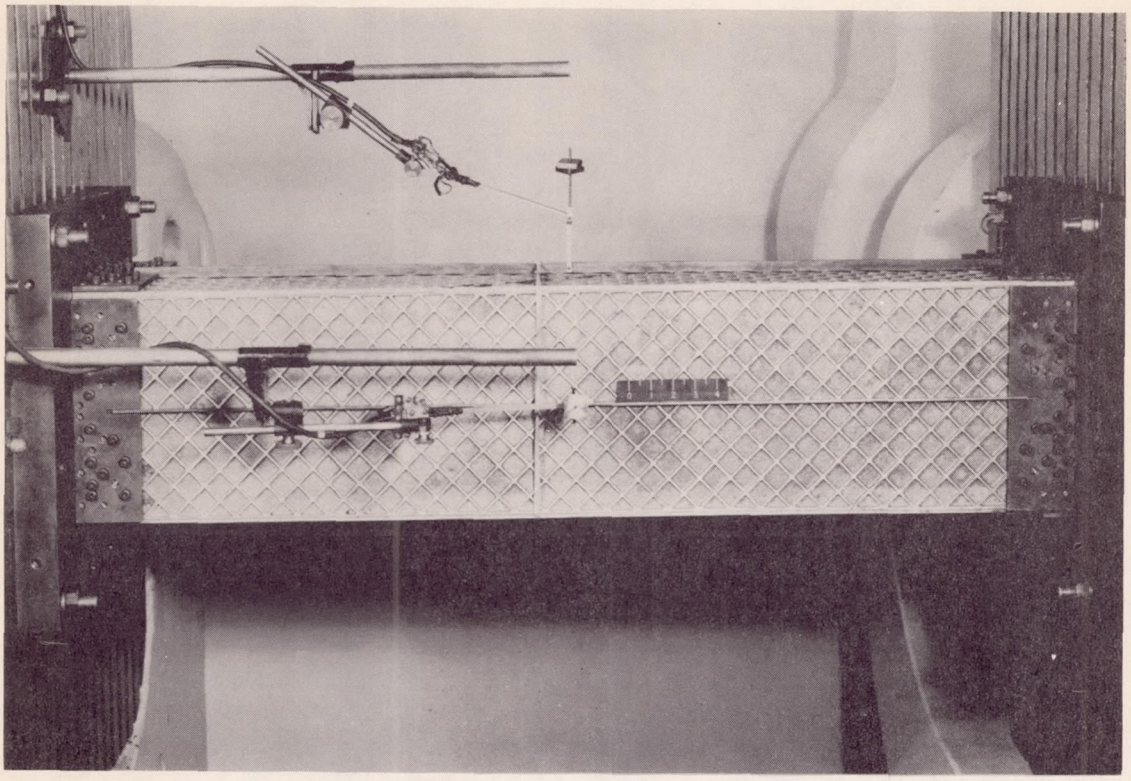

L-80893

Figure 3.- Arrangement for combined load test.

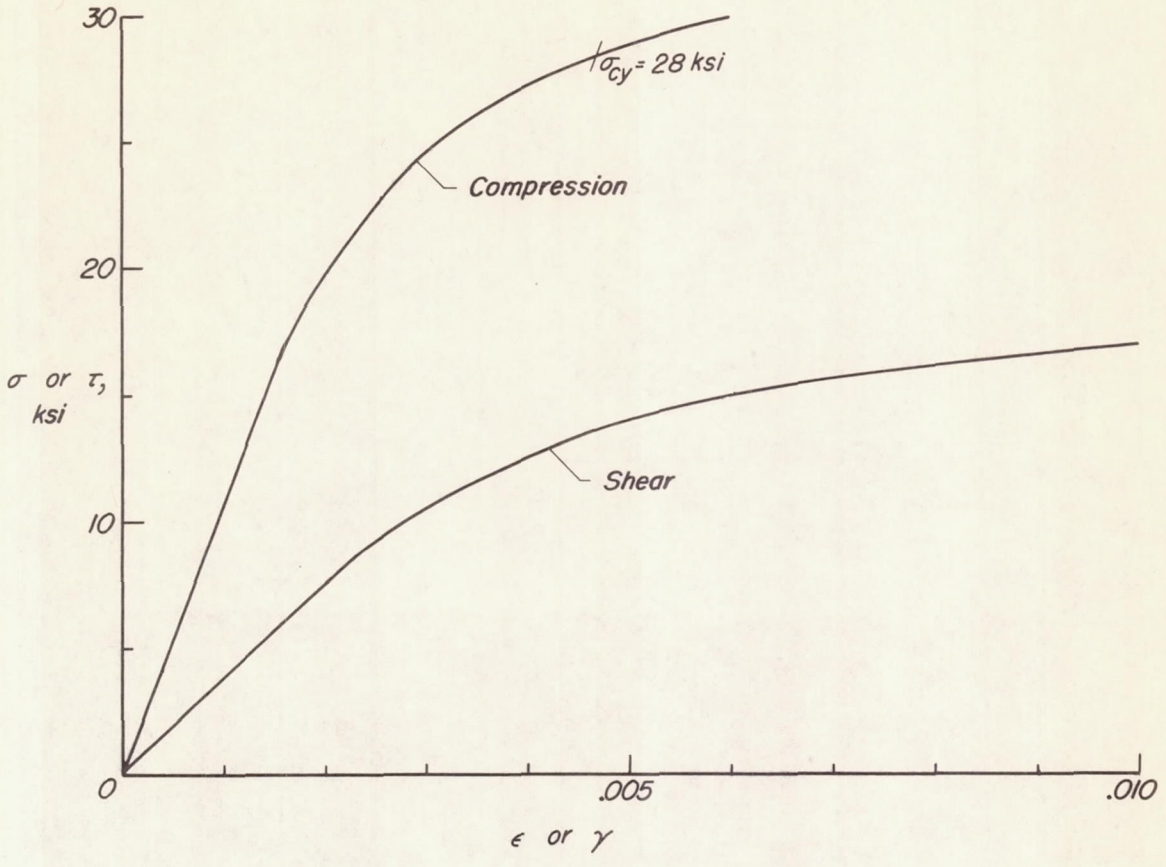

Figure 4.- Compression and shear stress-strain curves for 355-T61 aluminum alloy as used for test specimens.

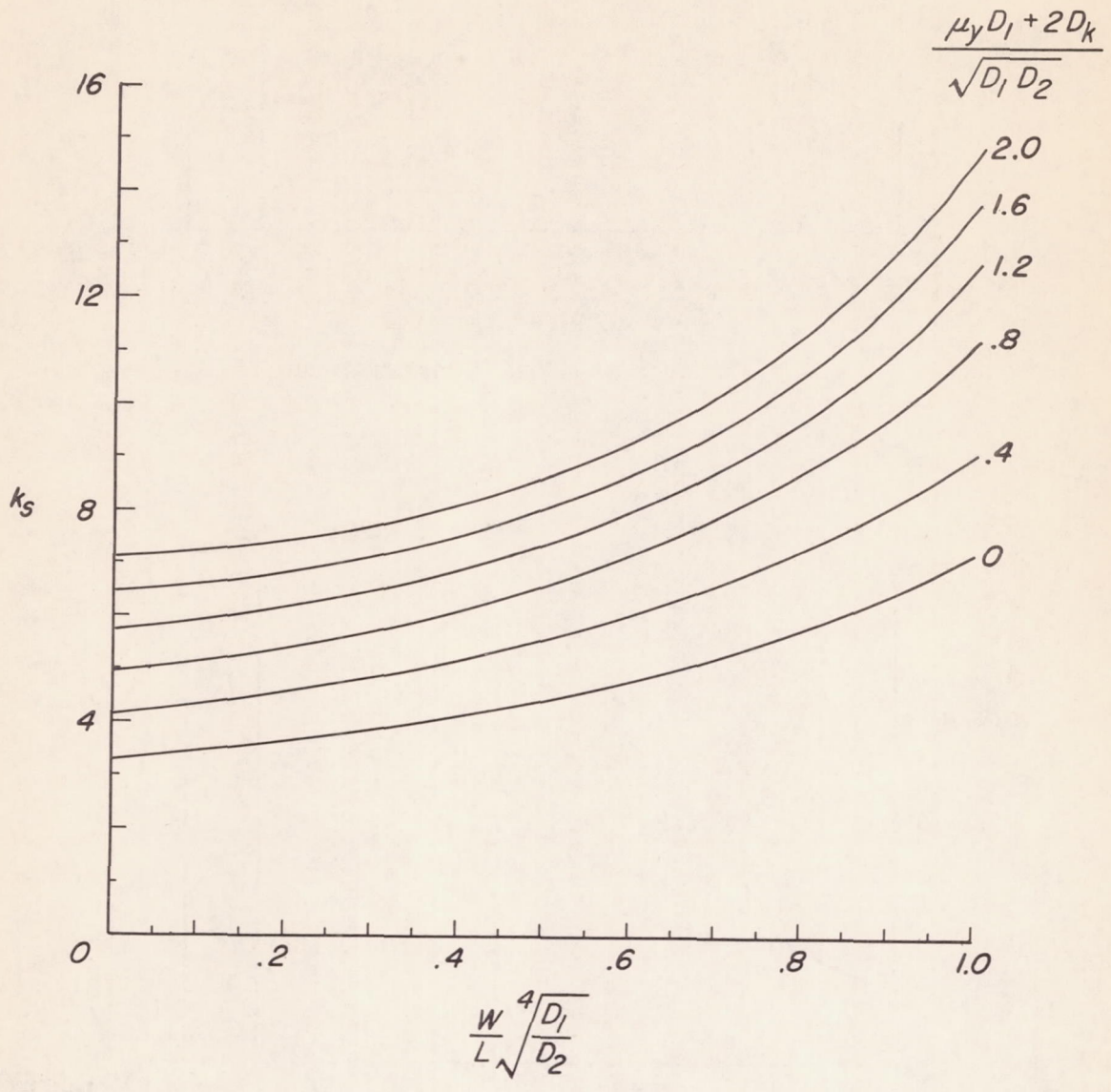

Figure 5.- Approximate values of k_S for orthotropic, rectangular plates clamped along the short edges and simply supported along the long edges.

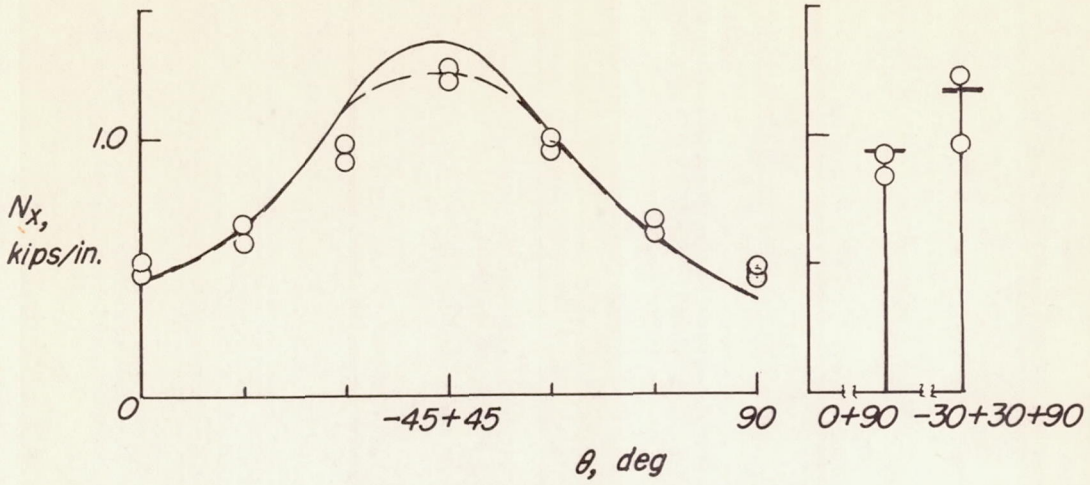

(a) Compression.

——— Elastic

— — — Plastic

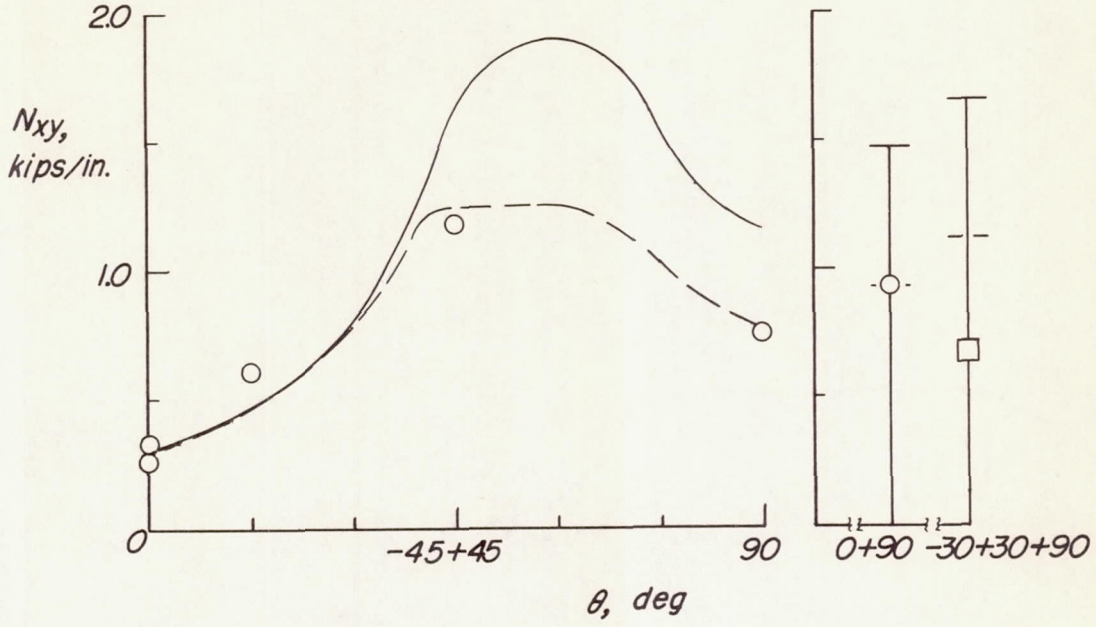

(b) Shear.

Figure 6.- Variation with angle of skew of ribbing of calculated and measured longitudinal compression and shear buckling loads.

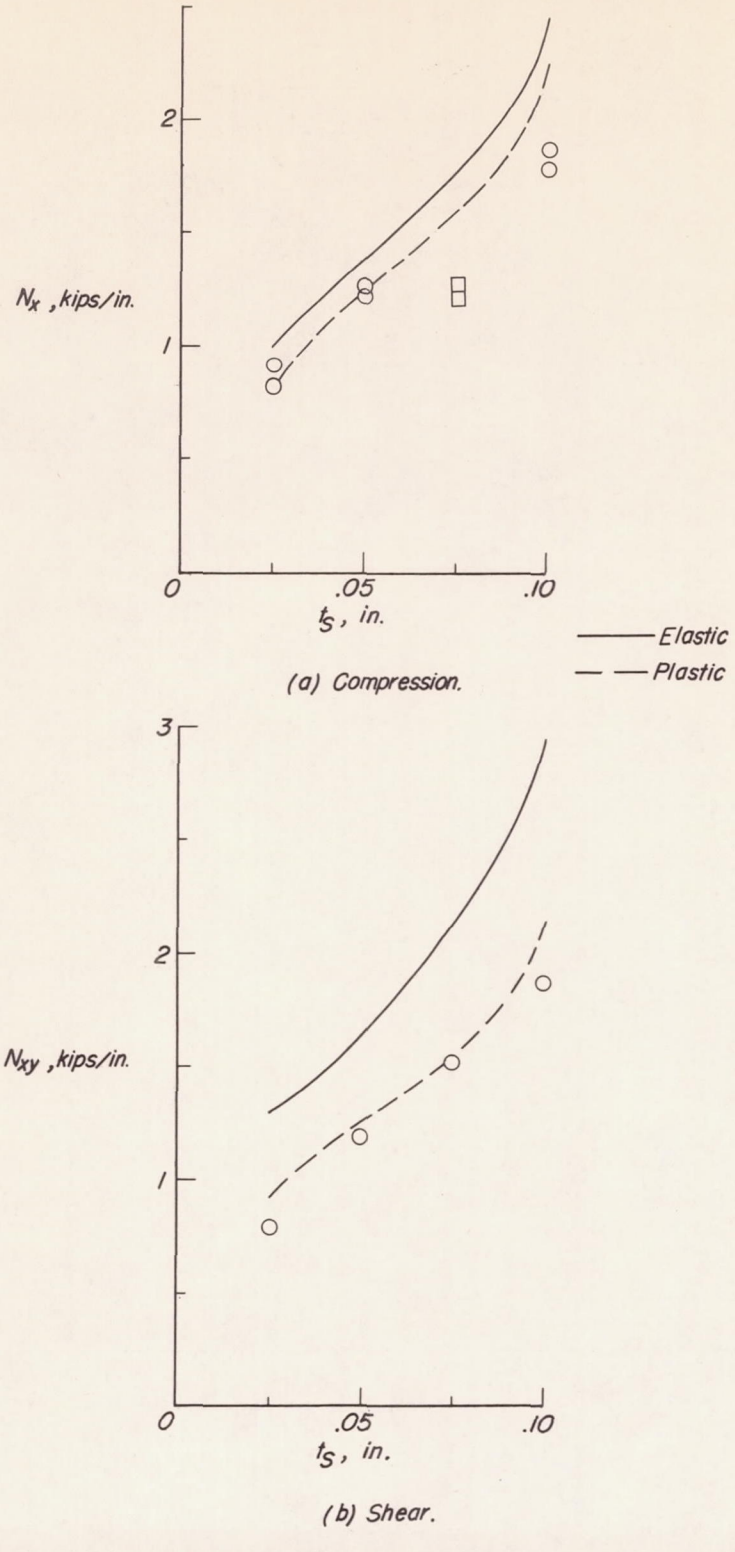

Figure 7.- Variation with skin thickness of calculated and measured longitudinal compression and shear buckling loads for -45° + 45° configuration.

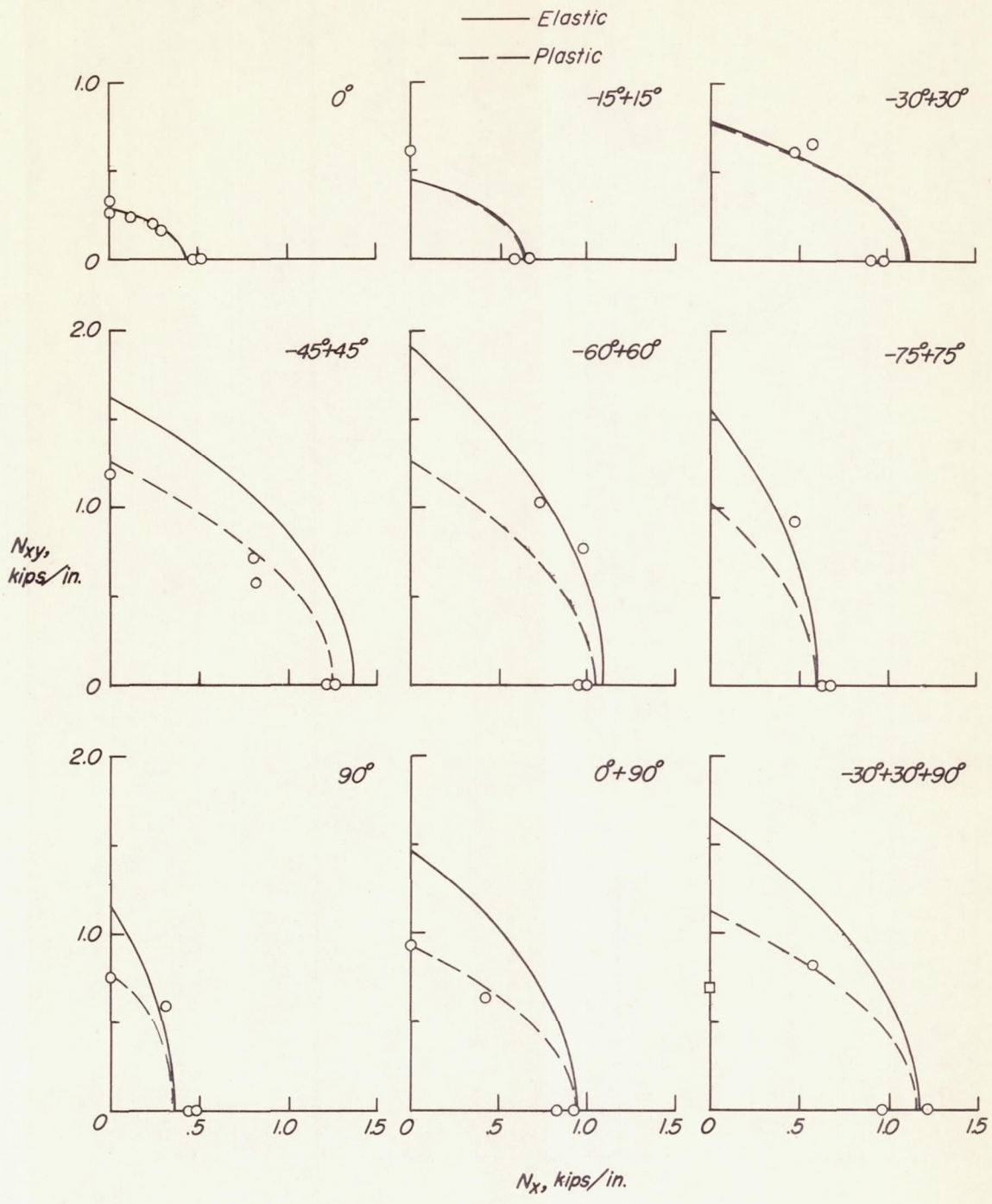

Figure 8.- Calculated and measured interaction curves for buckling under combined longitudinal compression and shear loads.

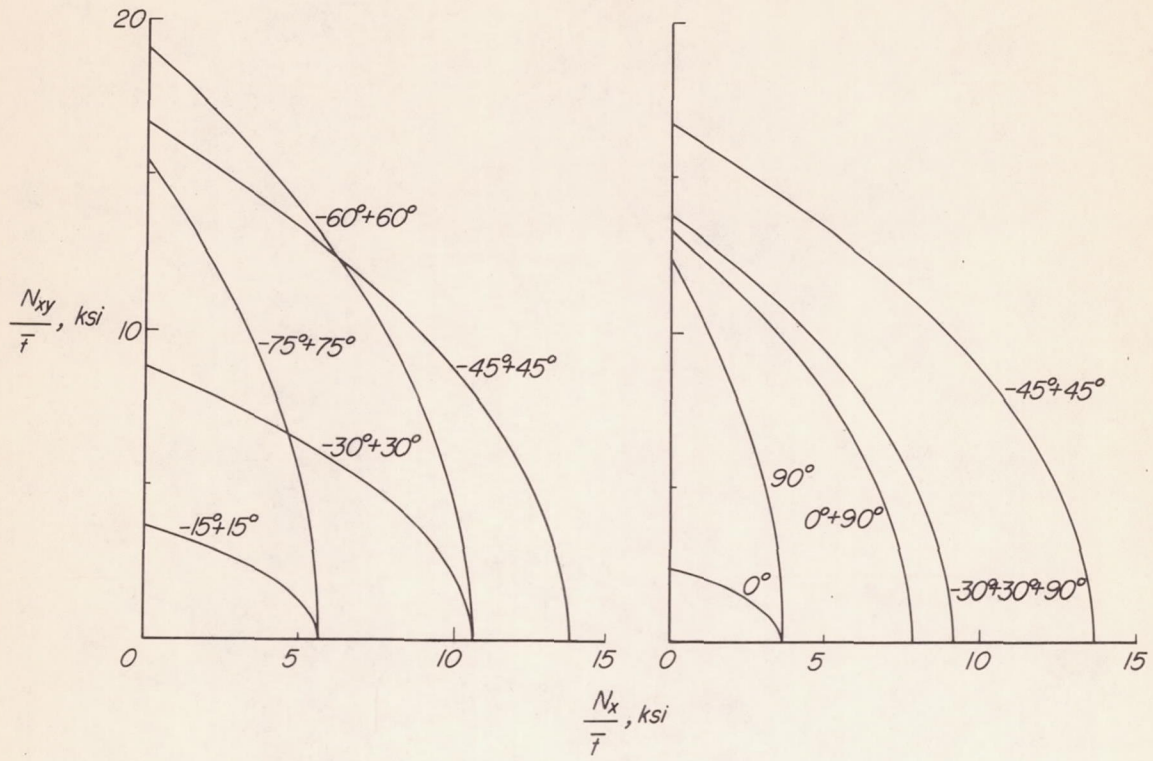

Figure 9.- Calculated elastic interaction curves for buckling under combined longitudinal compression and shear stresses of infinitely long simply supported integrally stiffened flat plates of the proportions investigated.